HIGH AND LOW CYCLE FATIGUE OF A 6060 ALUMINIUM ALLOY

LORENZO PAGLIARI[1], RICCARDO GEROSA[2], DAVIDE PANZERI[2] & FRANCO CONCLI[1]
[1]Faculty of Engineering, Free University of Bolzano, Italy
[2]Dipartimento di Meccanica, Politecnico di Milano, Italy

ABSTRACT

Lightweight alloys are gaining significant interest in light of their high strength-to-weight ratio, which paves the way to more efficient systems with a direct impact on pollutant emissions, sustainability and carbon footprint. The results of a High- (HCF) and Low-Cycle-Fatigue (LCF) characterization testing campaign performed on a 6060-Aluminium alloy are presented. The 6XXX-series aluminium alloys features Magnesium and Silicon. These alloying elements form Magnesium Silicide (Mg2Si) as strengthening phase. The two predominant components must maintain perfect proportions to create the Al-Mg-Si system. 6XXX-series alloys are most frequently used for extrusion, as they provide a good balance of strength, corrosion resistance, weldability, machinability, and surface finish. Understanding the exact mechanical behaviour is crucial for its large-scale adoption. A series of cylindrical samples, manufactured with traditional techniques, was used to determine the High-Cycle-Fatigue properties of the 6060-alloy exploiting the statistical approach proposed by Dixon. The maximum number of cycles (run-out) was set to 5000000. The finite-life range was also studied by means of additional tests at higher stress levels. Regarding the LCF, tests were carried out with a strain-ratio equal to -1. The fatigue data were studied by means of the Coffin-Manson-equation and the cyclic and static behaviours were compared. The 6XXX-Aluminum series do not normally exhibit elastic unstable fracture. These alloys are so tough that fracture toughness is rarely a design criterion. However, the present set of HCF samples exhibited intergranular fracture. This phenomenon occurs when cracks propagate along the grain boundaries when these are weakened, typically due to adverse environmental conditions or sensitization phenomena. In light of this evidence, the results were compared with data from literature. While the mechanical properties remain within the typical ranges, they are very low. Further analyses have been conducted to explain such poor mechanical behaviour, through the very unusual fracture mode that was observed.

Keywords: aluminium, high-cycle-fatigue, low-cycle-fatigue, intergranular fracture.

1 INTRODUCTION

The growing demand for increasingly high-performance systems has paved the way for the large-scale use of lightweight materials. Among these, aluminium is probably the most used, showing a constant growth throughout the years. Already in year 2000, aluminium alloys had overtaken plastic in the most-used-material ranking, becoming the third most widespread material in automobiles manufacturing. The success of aluminium alloys is mostly related to its extremely efficient production process.

The widespread and effective adoption of a material for new optimized components is strongly related to a deep knowledge of their properties. Apart from applications where gross yielding or high ductility fracture represents a limiting failure condition, tensile strength and yielding are insufficient requirements to design fracture-resistant structures. In addition to this, a separate chapter could be spent when dynamic loading is considered.

Achieving the project requirements necessitates considering severe stress concentrators, for which possible failure mechanisms may include high-cycle and low-cycle fatigue, brittle fracture, or even fracture from some combination of cyclic and static loading.

WIT Transactions on The Built Environment, Vol 216,
www.witpress.com, ISSN 1743-3509 (on-line)
doi:10.2495/HPSM250041

The proper alloy selection represents an important means of minimizing premature fracture in engineering structures but inevitably require a very deep knowledge of the material properties.

2 THE ALUMINIUM ALLOYS

Similar to other face-centred cubic materials, aluminium alloys usually do not experience a sudden ductile-to-brittle transition in fracture behaviour as temperatures decrease [1], [2]. Tensile test results show that nearly all aluminium alloys remain insensitive to strain rates ranging from 10^{-5} mm/mm/s to 1 mm/mm/s ($\approx 10^{-5}$ MPa/s) at both room and low temperatures [2]. Consequently, aluminium is well-suited for structural applications across a wide range of temperatures and loading conditions.

One possible classification of aluminium alloys is based on their strengthening mechanisms. Some alloys gain strength primarily through strain hardening (H), while others rely on solution heat treatment and precipitation aging (T). Another widely used classification, established by The Aluminium Association, identifies the primary alloying element by the first digit of the alloy designation.

The 1XXX series, for instance, is mostly pure Al, strengthened via cold working. The 2XXX series consists of a combination of Al-Cu-Mg, strengthened via heat treatments. The 3XXX series, is made up of Al-Mn-Mg (cold working), the 4XXX series consists of Al-Mg or Al-Mg-Mn (cold working), the 6XXX series consists of heat-treated Al-Mg-Si, the 7XXX series of heat-treated Al-Zn-Mg-(Cu), and the 8XXX series of heat treated Al-Li [3].

Among these, the 5XXX and 6XXX alloys provide medium-to-relatively high strength, excellent corrosion resistance, and exceptional toughness, making fracture toughness considerations generally unnecessary. The 6XXX series, focus of this work, is known for its good formability and weldability at moderate strengths and is widely applied in conventional structural projects. The typical range of tensile strength lies between 150 and 380 MPa.

3 6060-T6

This study focuses on a 6060 alloy (ISO designation AlMgSi). The EN-573-3:1994 foresee specific ranges for the alloying elements for the 6060 alloy. In particular, Si should be between 0.3 and 0.6, Fe between 0.1 and 0.3, Cu, Mn and Ti between 0 and 0.1, Mg between 0.35 and 0.6, Cr between 0 and 0.05 and Zn between 0 and 0.15.

For this specific alloy, limited data are available in literature. It usually undergoes a T6 heat treatment that foresees a heating process at very high temperatures (around 535°C), followed by a cooling step. The quenching is made in a liquid solution bath (usually water or glycol) at a temperature between 65°C and 100°C. After quenching, the castings are aged in a furnace, heated to 175°C for several hours and then allowed to cool naturally.

It has been shown that the T6 state increases the fatigue strength by approximately 30% compared to the T4 state [4]. Pisapia et al. [5] tested the 6060 aluminium alloy under different heat treatments under LCF loading and found that the 6060-T6 alloys exhibited high cyclic hardening behaviour. Hopperstad et al. [6] studied the uniaxial cyclic behaviour of the aluminium alloy 6060 in tempers T4 and T6. In the latter condition, the material exhibits cyclic softening. Comparison of corresponding hysteresis loops, shows that the effect of prior history is not very significant for temper T6. The scholars reported indications of the Bauschinger effect and the cyclic hardening in the form of the Chaboche model. Jha et al. [7] reported the properties of the 6060 aluminium alloy. The material was found to have high tensile strength (UTS = 374 MPa), yield strength (σ_Y = 303 MPa) and hardness. However, it is characterized by relatively low ductility.

In contrast, Fernandes et al. [8] reported quite low mechanical properties for the 6060-T6 alloy (σ_Y = 150 MPa, UTS = 190 MPa).

Despite these outliers, most of the records report values around 210 ÷ 230 MPa for what concerns the yielding and around 230 ÷ 250 MPa for that concern UTS.

Hockauf et al. [9] tested a 6060 alloy with different heat treatments. For its standard T6 version, the scholars reported a tensile strength of 233 MPa, and a yield strength of 208 MPa. Hockauf et al. reported also the high cycle fatigue properties in the form of Basquin coefficients ($b = -0.0787$, $\sigma_f^{'} = 354$ MPa). The scholars stated also that the crack growth threshold ΔK_{th} lies at 1.5 MPa·m$^{1/2}$. Moreover, Hockauf et al. [10] determined the influence of initial deformation on fatigue life and the effect of aging before cyclic fatigue. The proper fatigue tests were performed with the control of plastic strain amplitudes in the range $\varepsilon_{apl} = 1 \cdot 10^{-3} \div 5 \cdot 10^{-3}$. In addition to the determined fatigue characteristics in the stress–strain system, the resulting fatigue fractures were subjected to fractographic analysis.

Borrego et al. [11] performed LCF tests on 6060-T6 alloys subjected to strain ranges between 0.32% and 4%. They report a tensile strength of 240 MPa, and a yield strength of 215 MPa. The scholars include in their publication also the cyclic properties in the form of the Ramberg–Osgood (RO) coefficients ($k^{'} = 267.3$, $n^{'} = 0.38$). The tested alloy shows a brief initial cyclic hardening stage followed by long-term cyclic softening. Beside this, also the fatigue characteristics were presented in the form of Basquin–Coffin–Manson (BCM) coefficients ($b = -0.084$, $\sigma_f^{'} = 376.5$ MPa, $c = -0.537$, $\varepsilon_f^{'} = 0.157$).

The static characteristics were measured also by Corre et al. [12] (σ_Y = 229 ÷ 235 MPa, UTS = 251 ÷ 259 MPa). The scholars observed both transgranular ductile fracture with dimples, as expected for an aluminium alloy at room temperature, and intergranular ductile fracture, which is less common. Other scholars have already reported this type of fracture surfaces for aluminium alloys with a mixed mode failure [13], especially in Al-Mg-Si alloys [14]. In their study, the scholars observed a homogeneous fracture surface with no distinct features, consistent with the smaller amount of main precipitates (Mg_2Si hardening particles) and the complete absence of dispersoid phase. The observed nearly ideal Masing behaviour is coherent with the low level of precipitates and compatible with the Christ and Mughrabi hypothesis [15] (i.e. an important requirement for Masing-type behaviour in multiple-phase materials is that the particle/dislocation interaction is of minor importance for plastic deformation compared to dislocation interactions).

Kowalski et al. [16], [17] carried out a fractographic analysis of fatigue fracture surfaces of aluminium alloys after cyclic bending and torsion tests. Crack propagation occurs mainly by connecting successive cracks that are formed at adjacent grain boundaries. It was found that the microstructure, type, and size of cyclic loads determine the share of trans-crystalline, quasi-split, and ductile cracks, thus determining the fractography of fatigue samples.

4 EXPERIMENTAL SETUP

High-cycle-fatigue (HCF) tests were conducted on cylindrical specimens (Fig. 1 (left)) designed following the ASTM E466 standard [18]. The experiments were carried out using a STEPLab-UD04 fatigue testing machine, which can apply loads of up to 5 kN at a maximum frequency of 35 Hz. It was used for previous studies on aluminium alloys [19]–[21] as well as other materials [22], [23].

Alongside the HCF tests, quasi-static tensile characterization was performed. The geometry of the specimens used in these tests is depicted in Fig. 1 (left). Tensile testing was conducted at room temperature (20°C) with a crosshead speed of 0.1 mm/min. The fractured specimens exhibited a cone-cup shaped fracture surface, which is characteristic of ductile

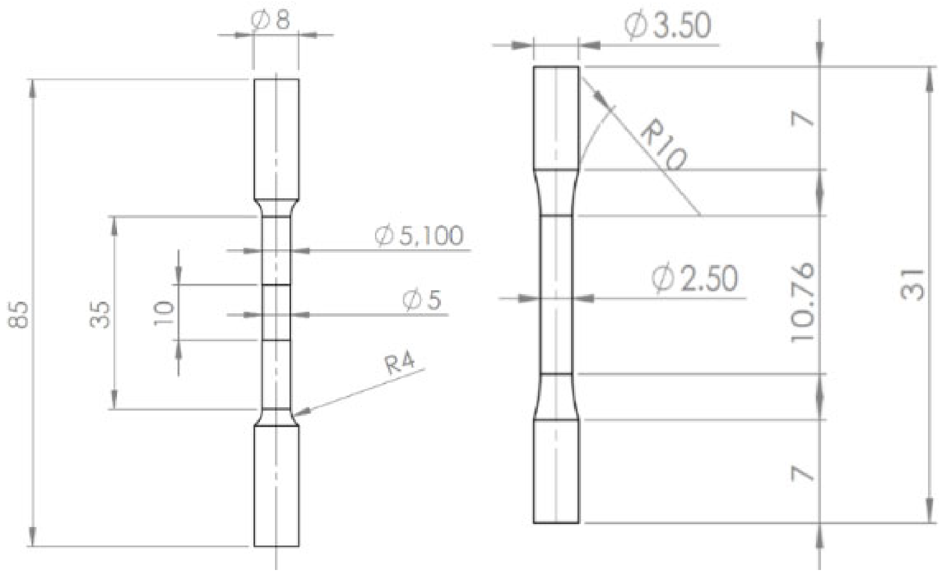

Figure 1: Standard specimen for quasi-static and HFC (left), according to ASTM E466 and LCF (right) tests according to ASTM E606.

failure. Additionally, plastic deformation was confirmed by the presence of a fibrous and irregular necking region.

Preliminary static tests were also carried out to determine the yield point (Fig. 2). The data obtained were subsequently used to calibrate the Basquin parameters, as detailed in the following sections.

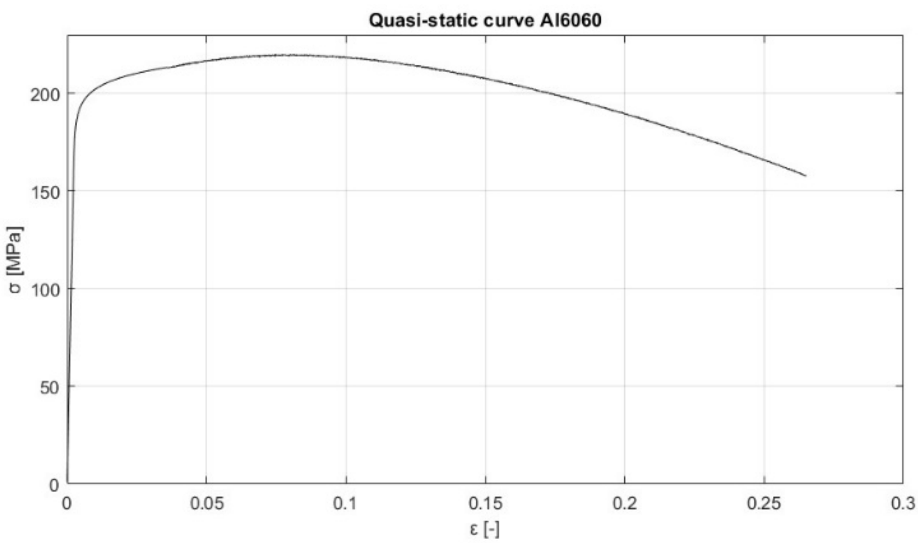

Figure 2: Quasi-static curve for the Al 6060.

4.1 HCF

HCF tests followed the ASTM E466 standard [18], and the fatigue limit was estimated using the short stair-case method [24]–[28]. Specifically, multiple tests were performed at varying load levels. This approach involves defining a force increment, which directly influences results accuracy. In this study, the increment was set at 50 N, corresponding to a stress interval ($\Delta\sigma$) of approximately 10.2 MPa.

If the initial test, conducted at a given force level, reached the run-out condition (5 million cycles without failure), the subsequent test was performed at a higher force level, increased by the defined increment. Conversely, if the specimen failed, the subsequent test was conducted at a lower force level, reduced by the same increment.

Fig. 3 illustrates the short stair-case sequences (five tests – the suggested value recommended by Dixon [24]) for the Al 6060 series. Unlike the conventional stair-case method, Dixon's statistical approach accounts not only for the number of failures (X) and run-outs (O) but also for the sequence order. A statistical correction coefficient ensures the reliability of the results.

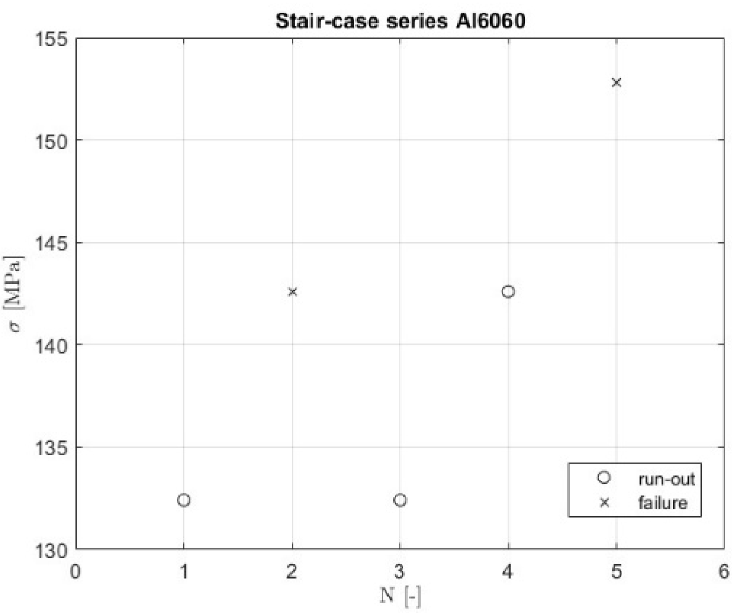

Figure 3: Results of the stair-case testing.

The fatigue limit was determined using the following equation:

$$\sigma_F = x_f + k \cdot \Delta\sigma, \tag{1}$$

where σ_F represents the fatigue limit at 50% probability, x_f denotes the stress level of the final test (ID = 5 in Fig. 3), and k is a sequence-dependent coefficient. The test sequence followed the order O-X-O-X-X, with a corresponding factor of −0.878. Based on this, the calculated fatigue limit was 143.8 MPa.

4.2 LCF

Low-cycle fatigue (LCF) tests were conducted on cylindrical specimens with standard dimensions in accordance with ASTM E606 [29], as depicted in Fig. 1 (right). Strain-controlled fatigue experiments were carried out using the STEPLab UD04 testing machine following the guidelines outlined in ASTM E606 [29]. The tests were performed at a specified strain ratio, with the testing frequency set at 0.1 Hz which represents the lowest frequency recommended by ASTM E606. This frequency remained constant throughout the tests, as increasing it could influence the results by slightly raising the sample temperature and altering its mechanical properties. The stabilized cycles for each deformation level were interpolated using the RO equation (eqn (2)) to derive the stabilized curves (Fig. 4).

$$\varepsilon_a = \varepsilon_{ae} + \varepsilon_{ap} = \frac{\sigma_a}{E} + \left(\frac{\sigma_a}{K'}\right)^{\frac{1}{n'}}. \quad (2)$$

In this equation, ε_a denotes the total strain amplitude, while ε_{ae} and ε_{ap} represent the elastic and plastic components, respectively. The stress amplitude is indicated by σ_a, and E corresponds to the elastic modulus. The constants K' and n' are material-dependent parameters [30]. It is important to note that these constants differ from those typically associated with the Hollomon equation [31]. The RO equation parameters are provided in Table 1.

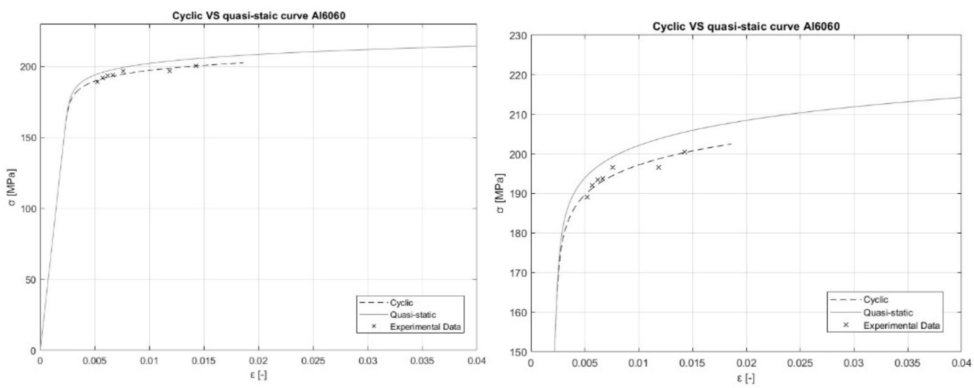

Figure 4: Cyclic vs. quasi-static curve (detail view on the right).

Table 1: RO parameters.

K′	**n′**
233.0807	0.0338

The Al 6060 exhibits softening behaviour. Even after stabilization, testing continued until sample failure to obtain data for fatigue curves, commonly referred to as BCM diagrams (eqn (3)):

$$\varepsilon_a = \frac{\Delta\varepsilon}{2} = \frac{\sigma_f'}{E}(2N)^b + \varepsilon_f'(2N)^c. \quad (3)$$

In this equation, σ_f', b, ε_f' and c represent four material-specific constants that need to be determined, namely the fatigue strength coefficient, the fatigue strength exponent, the fatigue ductility coefficient and the fatigue ductility exponent, respectively. Fig. 5 presents the experimental data obtained, along with the fitted curve using the BCM equation. The calculation process initially involves determining the Basquin coefficients based on the yield stress and high-cycle fatigue limit through linear interpolation. The Basquin equation, which describes the correlation between elastic deformation and the number of cycles, allows for the separation of plastic deformation from the total strain.

$$\varepsilon_{ap} = \varepsilon_a - \varepsilon_{ae} = \varepsilon_f^{'}(2N)^c. \tag{4}$$

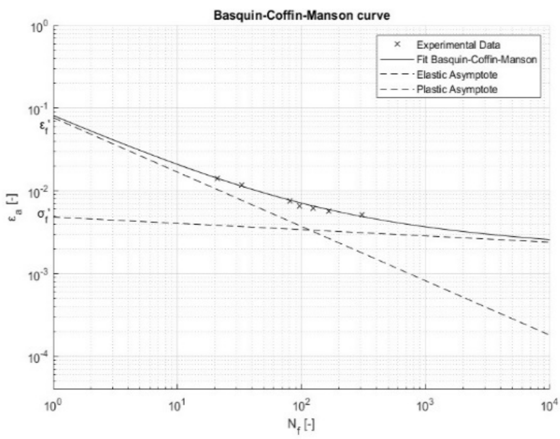

Figure 5: BCM curve.

To estimate the maximum likelihood parameters for b and c in accordance with eqn (4), the ASTM 739 standard [32] was considered. The equation for a best-fit line based on experimental data is expressed as follows:

$$\log(N) = \hat{A} + \hat{B}\log(\varepsilon_{ap}). \tag{5}$$

The maximum likelihood estimators for parameters A and B are given by $\hat{A} = \overline{Y} - \hat{B}\overline{X}$ and $\hat{B} = \frac{\sum(x_i - \overline{X})(y_i - \overline{Y})}{\sum(x_i - \overline{X})^2}$, where $\overline{X}$ and $\overline{Y}$ represent the average values of the independent x_i ($\log(\varepsilon_{ap})$) and independent variable y_i ($\log(N)$).

Eqn (5) can be reformulated as follows:

$$\varepsilon_{ap} = 10^{-\frac{\hat{A}}{\hat{B}}}\left(\frac{1}{2}\right)^{\frac{1}{\hat{B}}}(2N)^{\frac{1}{\hat{B}}}. \tag{6}$$

Thus, the maximum likelihood estimators for the Coffin–Manson coefficients, c and $\varepsilon_f^{'}$ can be expressed as:

$$\varepsilon_f^{'} = 10^{-\frac{\hat{A}}{\hat{B}}}\left(\frac{1}{2}\right)^{\frac{1}{\hat{B}}} \tag{7}$$

$$c = 1/\hat{B} \tag{8}$$

The final computed values are provided in Table 2.

Table 2: BCM coefficients.

σ'_f (MPa)	b	ε'_f	c
351.9	−0.076	0.121	−0.657

5 EXPERIMENTAL SETUP

Some samples were cut from the tested specimens to observe the microstructural characteristics. After the standard metallographic preparation by mounting the specimens in a cold-setting resin and by mirror polishing, the samples were observed after the chemical etching (Keller’s and Weck’s reagents).

Fig. 6 shows the observed microstructure by light optical and scanning electron microscopes (LOM and SEM, respectively). Polygonal grains were clearly visible in both the LOM and SEM images. The average grain size is about 43 µm. The particles remarked in Fig. 6(d) were analysed by EDS probe. They are Fe-rich phases as reported in Table 3.

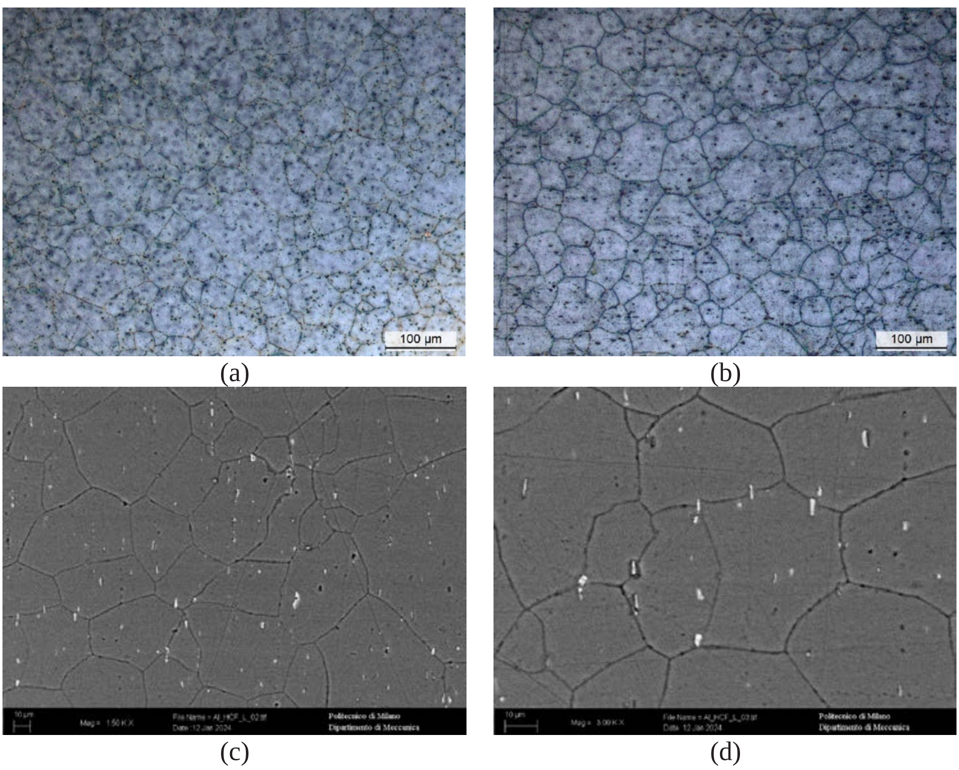

Figure 6: Metallographic analysis of the investigated samples. (a) Transversal HCF section, LOM; (b) Longitudinal HCF section, LOM; (c) Longitudinal HCF section, SEM; (d) Magnification of (c).

Table 3: EDS analyses on the particles remarked in Fig. 7(a).

	Mg (%)	Si (%)	Fe (%)
A	0.65	3.10	6.60
B	0.50	4.63	12.39
C	0.35	3.09	4.36

6 ANALYSIS OF THE FRACTURE SURFACES

Figs 7 and 8 show the fracture surfaces of some of the tested HCF and LCF specimens. In the nucleation zone, an intergranular fracture can be seen. It is an infrequent mechanism that can be related to the precipitation of Mg-Si rich particles at grain boundary. Li et al. [33] reported that such kind of failure can occur in ductile metals only under particular conditions of temperature, strain rate and interstitial atoms content. As confirmed by other authors [34]–[37], it is believed that fatigue cracking can be generated at grain boundaries when persistent slip bands (PSBs) are blocked by grain boundaries creating a stress concentration. Moreover, the presence of intermetallic phases such as Mg-Si precipitates can enhance the formation of the first micro-voids.

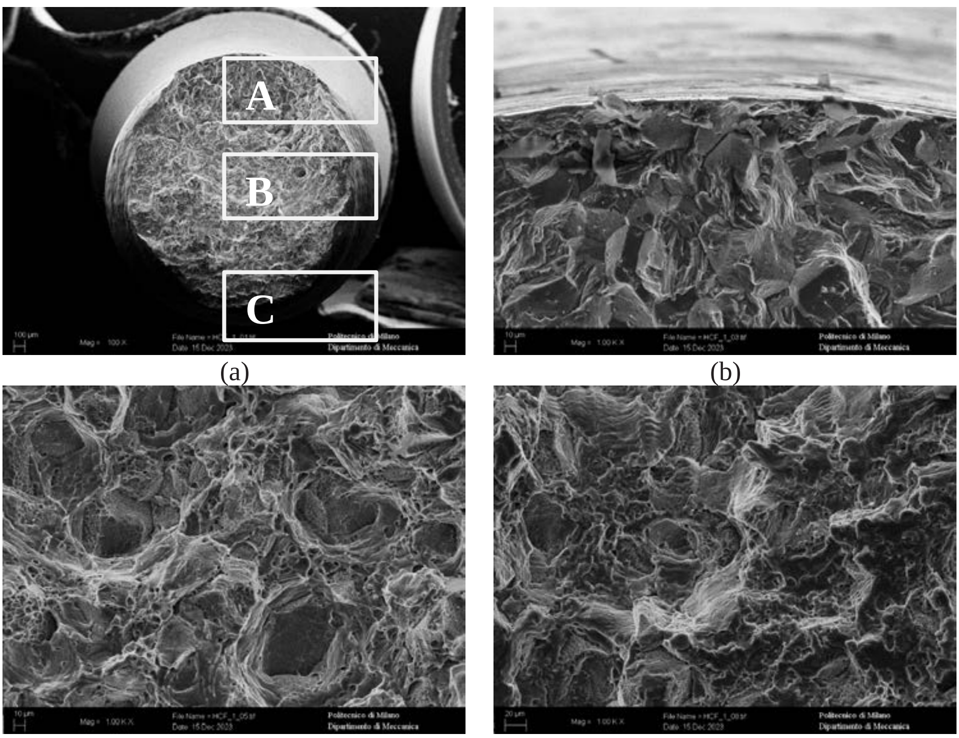

Figure 7: Fracture surface of one HCF specimen. Zone A represents the nucleation zone. The crack propagates downward across zones B and C. Pictures (b), (c) and (d) are magnifications of Zones A, B and C respectively.

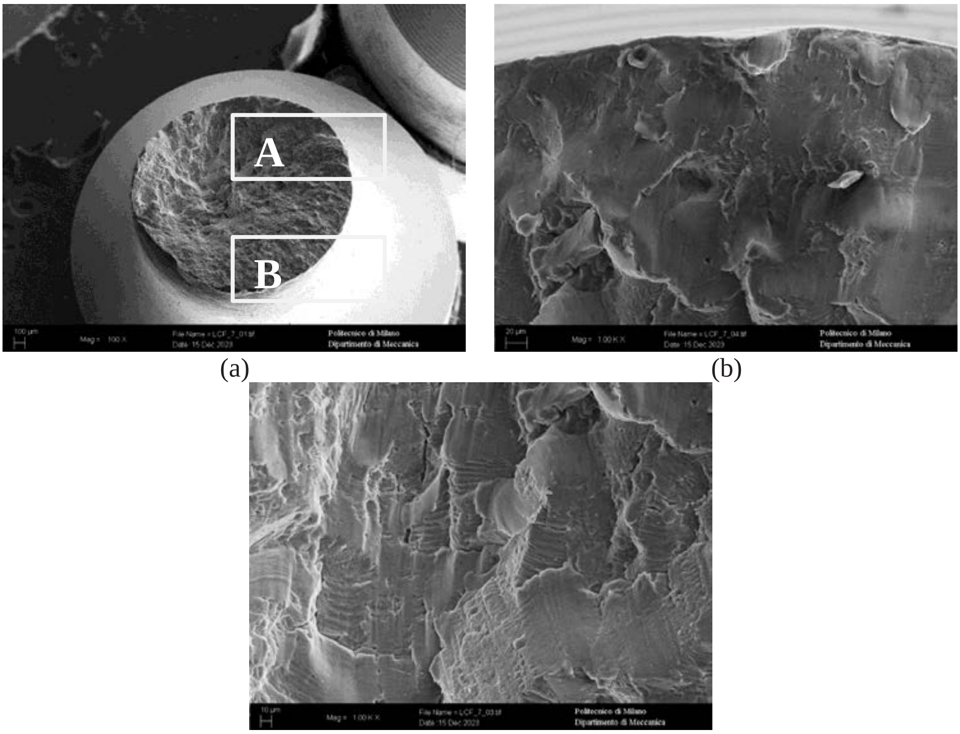

(a) (b) (c)

Figure 8: Fracture surface of one LCF specimen. Zone A represents the nucleation zone. The crack propagates downward across zones B. (b) and (c) are magnifications of Zones A and B, respectively.

The intergranular characteristic is less visible in Zone B and disappear in Zone C. In zones B and C dimples and some striations can be observed as well.

The LCF fracture surfaces are more complicated to be studied since some damages are present probably because of the higher loads and of the load ratio ($R = -1$). No intergranular feature can be seen, but it can be hidden by the local deformations visible in Fig. 8. Nevertheless, striations are clearly visible in Fig. 8(c).

7 CONCLUSIONS

In this work an Al 6060 alloy was tested under static and dynamic loadings.

The quasi-static test allows the determination of the elastic modulus and the ultimate tensile stress (69 GPa and 219 MPa, respectively). These values are aligned with the findings of other scholars.

Fatigue tests were performed under both low-cycle and high-cycle-fatigue conditions. The cyclic behaviour was modelled via the RO model showing a marked softening behaviour. The high-cycle-fatigue limit was determined exploiting the short stair-case approach proposed by Dixon, resulting in 143.8 MPa. The strain–cycle curve was interpolated using the BCM model. The results are aligned with the finding of other scholars.

The peculiarity of this research is in the observed fracture mechanism. In particular, an intergranular fracture was observed. It is an occasional mechanism related to the precipitation of Mg-Si rich particles at grain boundary that can occur in ductile metals only under particular conditions of temperature, strain rate and interstitial atoms content.

REFERENCES

[1] Kaufman, J.G. & Holt, M., Fracture characteristics of aluminum alloys. Technical paper no. 18, Aluminum Company of America, Pittsburgh, PA, 48 pp., 1965.

[2] Kaufman, J.G., Aluminum alloys for Arctic applications. *Proceedings of the Conference on Materials Engineering in the Arctic*, St. Jovite, Quebec, 1976.

[3] Bucci, R.J., Selecting aluminum alloys to resist failure by fracture mechanisms. *Eng. Fract. Mech.*, **12**, pp. 407–441, 1979.

[4] Wagener, R. & Melz, T., Fatigue life curve: A continuous Wöhler curve from LCF to VHCF: Dedicated to Professor Dr. Ing. Harald Zenner on the occasion of his eightieth birthday. *Materials Testing*, **60**, pp. 924–930, 2018.

[5] Pisapia, A., Nastri, E., Piluso, V., Formisano, A. & Mazzolani, F.M., Experimental campaign on structural aluminium alloys under monotonic and cyclic loading. *Eng. Struct*., **282**, 115836, 2023.

[6] Hopperstad, O.S., Langseth, M. & Remseth, S., Cyclic stress–strain behaviour of alloy AA6060, Part I: Uniaxial experiments and modelling. *Int. J. Plast*., **11**, pp. 725–739, 1995.

[7] Jha, S.K., Balakumar, D. & Paluchamy, R., Experimental analysis of mechanical properties on AA6060 and 6061 aluminum alloys. *Int. J. Eng. Res. Appl*., **5**, pp. 47–53, 2015.

[8] Fernandes, F.A.O., Gonçalves, J.J.M. & Pereira, A.B., Evaluation of laser lap weldability between the titanium alloy Ti-6Al-4V and aluminum alloy 6060-T6. *Crystals (Basel)*, **13**, p. 1448, 2023.

[9] Hockauf, K., Meyer, L.W., Halle, T. & Hockauf, M., Rissfortschritts-und ermüdungsverhalten der aluminiumlegierung EN AW-6060 nach ECAP und nachgelagerter wärmebehandlung. *Materialwissenschaft und Werkstofftechnik: Entwicklung, Fertigung, Prüfung, Eigenschaften und Anwendungen Technischer Werkstoffe*, **40**, pp. 493–499, 2009.

[10] Hockauf, K., Niendorf, T., Wagner, S., Halle, T. & Meyer, L.W., Cyclic behavior and microstructural stability of ultrafine-grained AA6060 under strain-controlled fatigue. *Procedia Eng*., **2**, pp. 2199–2208, 2010.

[11] Borrego, L.P., Abreu, L.M., Costa, J.M. & Ferreira, J.M., Analysis of low cycle fatigue in AlMgSi aluminium alloys. *Eng. Fail. Anal*., **11**, pp. 715–725, 2004.

[12] Corre, T., Perrin, J., Gebhard, J., Duchateau, T., Lilensten, L., Laurent-Brocq, M., Tekkaya, A.E. & Huneau, B., Tensile and shear behavior of recycled AA 6060 aluminium chips by direct hot extrusion. *Materials Science and Technology*, 02670836241287768, 2024.

[13] Pardoen, T., Dumont, D., Deschamps, A. & Brechet, Y., Grain boundary versus transgranular ductile failure. *J. Mech. Phys. Solids*, **51**, pp. 637–665, 2003.

[14] Prince, K.C. & Martin, J.W., The effects of dispersoids upon the micromechanisms of crack propagation in Al Mg Si alloys. *Acta Metallurgica*, **27**, pp. 1401–1408, 1979.

[15] Christ, H.-J. & Mughrabi, H., Cyclic stress–strain response and microstructure under variable amplitude loading. *Fatigue Fract. Eng. Mater. Struct.*, **19**, pp. 335–348, 1996.

[16] Kowalski, A., Ozgowicz, W., Jurczak, W., Grajcar, A., Boczkal, S. & Kurek, A., Microstructural and fractographic analysis of plastically deformed Al-Zn-Mg alloy subjected to combined high-cycle bending-torsion fatigue. *Metals (Basel)*, **8**, p. 487, 2018.

[17] Kowalski, A., Ozgowicz, W., Grajcar, A., Lech-Grega, M. & Kurek, A., Microstructure and fatigue properties of AlZn6Mg0. 8Zr alloy subjected to low-temperature thermomechanical processing. *Metals (Basel)*, **7**, p. 448, 2017.
[18] ASTM, Standard Practice for Conducting Force Controlled Constant Amplitude Axial Fatigue Tests of Metallic Materials. ASTM, 2007.
[19] Concli, F. & Gilioli, A., Numerical and experimental assessment of the static behavior of 3D printed reticular Al structures produced by selective laser melting: progressive damage and failure. *Proceedings of the Procedia Structural Integrity*, **12**, pp. 204–212, 2018.
[20] Concli, F., Gilioli, A. & Nalli, F., Experimental–numerical assessment of ductile failure of additive manufacturing selective laser melting reticular structures made of Al A357. *Proc. Inst. Mech. Eng. C. J. Mech. Eng. Sci.*, **235**, pp. 1909–1916, 2021.
[21] Nalli, F., Cortese, L. & Concli, F., Ductile damage assessment of Ti6Al4V, 17-4PH and AlSi10Mg for additive manufacturing. *Eng. Fract. Mech.*, **241**, 2021.
[22] Alomar, Z. & Concli, F., Compressive behavior assessment of a newly developed circular cell-based lattice structure. *Mater. Des.*, **205**, 2021.
[23] Concli, F. & Gilioli, A., Numerical and experimental assessment of the mechanical properties of 3D printed 18-Ni300 steel trabecular structures produced by selective laser melting: A lean design approach. *Virtual Phys. Prototyp.*, **14**, pp. 267–276, 2019.
[24] Dixon, W.J., The up-and-down method for small samples. *J. Am. Stat. Assoc.*, **60**, pp. 967–978, 1965.
[25] Gorla, C. et al., Bending fatigue strength of case carburized and nitrided gear steels for aeronautical applications. *International Journal of Applied Engineering Research*, **12**, pp. 11306–11322, 2017.
[26] Concli, F., Austempered ductile iron (ADI) for gears: Contact and bending fatigue behavior. *Procedia Structural Integrity*, **8**, pp. 14–23, 2018.
[27] Gorla, C., Conrado, E., Rosa, F. & Concli, F., Contact and bending fatigue behaviour of austempered ductile iron gears. *Proc. Inst. Mech. Eng. C. J. Mech. Eng. Sci.*, **232**, pp. 998–1008, 2018.
[28] Gorla, C., Rosa, F., Concli, F. & Albertini, H., Bending fatigue strength of innovative gear materials for wind turbines gearboxes: Effect of surface coatings. *Proceedings of the ASME International Mechanical Engineering Congress and Exposition*, **45233**, pp. 3141–3147, 2012.
[29] ASTM, Standard Test Method for Strain-Controlled Fatigue Testing. ASTM E606/E606M, ASTM International, 2012.
[30] Ramberg, W. & Osgood, W.R., *Description of Stress–Strain Curves by Three Parameters*, 1943.
[31] Hollomon, J.H., Tensile deformation. *Aime Trans*, **12**, pp. 1–22, 1945.
[32] ASTM, Standard Practice for Statistical Analysis of Linear or Linearized Stress-Life (s–n) and Strain-Life (e–n) Fatigue Data. ASTM 739-91, 2006.
[33] Li, Y., Qiu, S., Zhu, Z., Han, D., Chen, J. & Chen, H., Intergranular crack during fatigue in Al-Mg-Si aluminum alloy thin extrusions. *Int. J. Fatigue*, **100**, pp. 105–112, 2017.
[34] Islam, M.N. & Arai, Y., Ultrasonic back reflection evaluation of crack growth from PSBs in low-cycle fatigue of stainless steel under constant load amplitude. *Materials Science and Engineering: A*, **520**, pp. 49–55, 2009.
[35] Essmann, U., Gösele, U. & Mughrabi, H., A model of extrusions and intrusions in fatigued metals I. Point-defect production and the growth of extrusions. *Philosophical Magazine A*, **44**, pp. 405–426, 1981.

[36] Taheri, S., Hauet, A., Taleb, L. & Kpodekon, C., Micro–macro investigations about the fatigue behavior of pre-hardened 304L steel. *Int. J. Plast.*, **27**, pp. 1981–2004, 2011.
[37] James, M.N., Intergranular crack paths during fatigue in interstitial-free steels. *Eng. Fract. Mech.*, **77**, pp. 1998–2007, 2010.